A Myoglobin Mutant Designed to Mimic the Oxygen-Avid *Ascaris suum* Hemoglobin: Elucidation of the Distal Hydrogen Bonding Network by Solution NMR

Wei Zhang,* Francesca Cutruzzolá,# Carlo Travaglini Allocatelli,# Maurizio Brunori,# and Gerd N. La Mar*
*Department of Chemistry, University of California, Davis, California 95616 USA, and #Dipartimento di Scienze Biochimiche "A. Rossi Fanelli" and Centro di Biologia Molecolare CNR, I-00185 Rome, Italy

ABSTRACT The solution ^{1}H NMR structure of the active site and ligand dissociation rate for the cyanomet complex have been determined for a sperm whale myoglobin triple mutant Leu29(B10)→Tyr, His64(E7)→Gln, Thr67(E10)→Arg that mimics the distal residue configuration of the oxygen-avid hemoglobin from *Ascaris suum*. A double mutant that retains Leu29(B10) was similarly investigated. Two-dimensional NMR analysis of the iron-induced dipolar shifts, together with the conserved proximal side structure for the two mutants, allowed the determination of the orientations of the paramagnetic susceptibility tensor for each complex. The resulting magnetic axes, together with paramagnetic relaxation and steady-state NOEs, led to a quantitative description of the distal residue orientations. The distal Tyr29(B10) in the triple mutant provides a strong hydrogen bond to the bound cyanide comparable to that provided by His64(E7) in wild-type myoglobin. The distal Gln64(E7) in the triple mutant is sufficiently close to the bound cyanide to serve as a hydrogen bond donor, but the angle is not consistent with a strong hydrogen bond. Dipolar contacts between the Arg67(E10) guanidinium group and the Gln64(E7) side chain in both mutants support a hydrogen-bond to the Gln64(E7) carbonyl group. The much lower oxygen affinity of this triple mutant relative to that of *Ascaris* hemoglobin is concluded to arise from side-chain orientations that do not allow hydrogen bonds between the Gln64(E7) side-chain NHs and both the ligand and Tyr29(B10) hydroxyl oxygen. Cyanide dissociation rates for the reduced cyanide complexes are virtually unaffected by the mutations and are consistent with a model of the rate-determining step as the intrinsically slow Fe-C bond breaking that is largely independent of any hydrogen bonds to the cyanide nitrogen.

INTRODUCTION

One of the major protein interactions that stabilize the Fe-O_2 bond in myoglobin (Mb) and hemoglobin (Hb) is a hydrogen bond by a distal residue to the bound O_2 molecule (Philips and Schoenborn, 1981; Shaanan, 1983; Perutz, 1989; Olson et al., 1988). In the more extensively studied mammalian Mbs, the residue in position E7 (residue 7 on helix E out of eight helices A-H) is ubiquitous in providing the hydrogen bond, most frequently by a His, but also by Gln (Dene et al., 1980; Sharma et al., 1987). The E7 residue is occupied by a broader range of residues in invertebrate Hbs and Mbs (Moens et al., 1996), and hydrogen bonding to the bound ligand in some cases is achieved via residues at other helical positions. Two striking examples are *Aplysia limacina* Mb, which possesses a Val E7, and in which residue Arg E10 extends into the pocket and provides a hydrogen bond to the ligand (Bolognesi et al., 1989, 1990; Cutruzzolá et al., 1996), and *Ascaris suum* Hb, which possesses the unusual residue Tyr B10, which provides an extra hydrogen bond (De Baere et al., 1994; Kloek et al., 1994; Yang et al., 1995; Huang et al., 1996). The stabilizing influence of a Tyr B10 can be viewed with surprise, because mutations of E7 His→Tyr in human HbA invariably result in oxidation of the heme iron and thereby inactivation of the O_2 carrier (Antonini and Brunori, 1971; Bunn and Forget, 1986). *Ascaris* Hb is unique in exhibiting an extraordinarily high oxygen affinity by virtue primarily of the slowest known O_2 off rate among all Mbs and Hbs (Davenport, 1949; Gibson and Smith, 1965; De Baere et al., 1994). The crystal structure of the expressed domain of the *Ascaris* chimeric Hb reveals a Tyr B10 appropriately oriented to hydrogen bond to the bound O_2, with the distal Gln E7 possibly providing a second hydrogen bond (De Baere et al., 1994; Kloek et al., 1994; Yang et al., 1995). Moreover, Gln E7 and Tyr B10 participate in an interresidue hydrogen bond that indirectly contributes to the strength of the Tyr B10 hydrogen bond to O_2 by stabilizing the appropriate orientation of the latter side chain.

We generated by mutagenesis a new sperm whale Mb triple mutant, Leu29(B10)→Tyr, His64(E7)→Gln, Thr67(E10)→Arg (identified as L29Y|H64Q|T67R-Mb), designed to mimic the distal pocket of *Ascaris* Hb. This mutant displays an O_2 affinity much lower, and an O_2 off rate much faster, than those of *Ascaris* Hb; nevertheless, relative to the double mutant, H64Q|T67R-Mb, incorporation of Tyr29(B10)resulted in an increased O_2 affinity and decreased O_2 off rate (by ~100-fold), indicating that Tyr B10 can serve as a hydrogen-bond donor to O_2 in the triple mutant Mb, albeit much less efficiently than in *Ascaris* Hb (Travaglini Allocatelli et al., 1994). The question that arises is whether Tyr B10 and Gln E7 in the triple-mutant Mb are

Received for publication 3 February 1997 and in final form 7 May 1997.
Address reprint requests to Dr. Gerd N. La Mar, Department of Chemistry, University of California, Davis, CA 95616. Tel.: 916-752-0958; Fax: 916-752-8995; E-mail: lamar@indigo.ucdavis.edu.

0006-3495/97/08/1019/12 $2.00

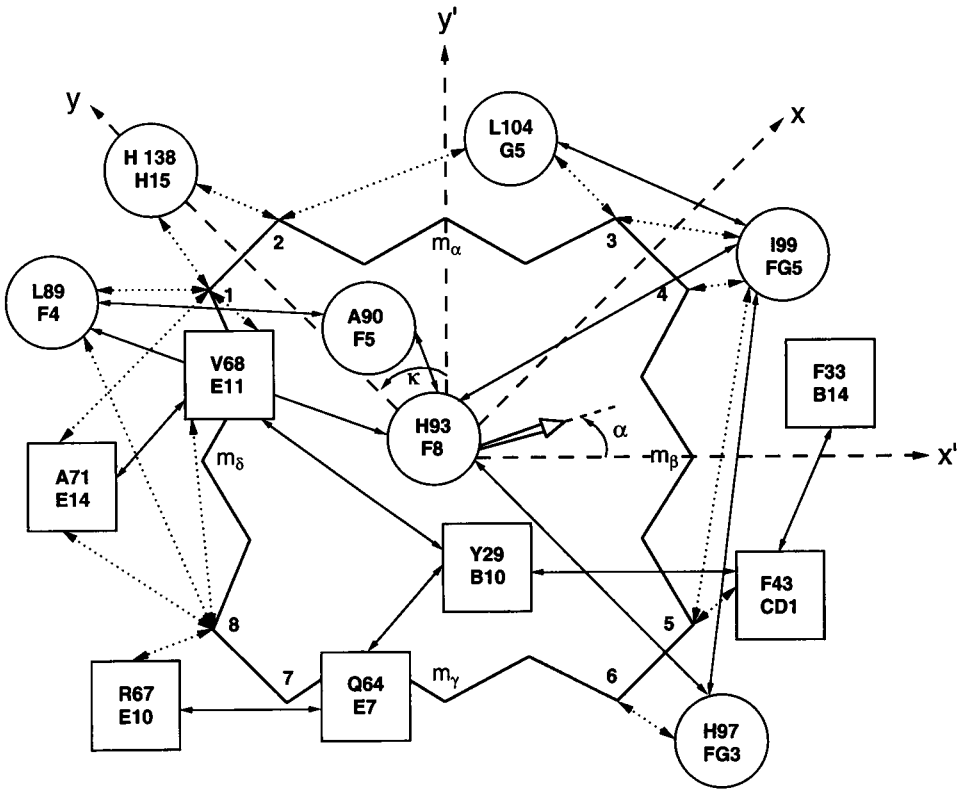

FIGURE 1 Schematic representation of the heme pocket structure of sperm whale Mb with face-on view from the proximal side. The hemin substituents are labeled M (methyl), V (vinyl), and P (propionate). Proximal and distal residues are represented as circles and squares, respectively. The double-sided arrows represent inter-residue and residue-heme dipolar contacts observed in L29Y|H64Q|T67R-metMbCN. Also shown is the definition of the magnetic axes x, y, z relative to the iron-centered crystal coordinates x', y', z'. The two coordinate systems are related by the standard Euler rotation $\Gamma(\alpha, \beta, \gamma)$, where $[x, y, z] = [x', y', z']\Gamma(\alpha, \beta, \gamma)$. The tilt of the major magnetic or z axis from the heme normal is given by β, where α is the angle between the projection of the z axis tilt on the heme plane and the x' axis.

capable of forming the same hydrogen-bonding pattern as in *Ascaris* Hb, even if stabilization of bound O_2 is less pronounced, or whether these interactions are significantly different in the mutant Mb relative to *Ascaris* Hb.

To answer these questions, we have selected for NMR study the paramagnetic cyanomet L29Y|H64Q|T67R-Mb and H64Q|T67R-Mb derivatives, in part because they are much more stable than the oxy complexes, but also because cyanide, like O_2, is a hydrogen-bond acceptor and hence can serve as a model for the hydrogen-bonding pattern in MbO_2. Moreover, the intrinsic paramagnetism of the low-spin ferric complex provides the resolution via hyperfine shifts to readily locate, assign, and spatially define not only the side chains for the key distal residues, but also the labile protons in the putative hydrogen-bonding network. The disposition of the key residues relative to each other and to the heme, and their individual protons, can be described by both conventional nuclear Overhauser effect/nuclear Overhauser spectroscopy (NOE/NOESY) contacts, as well as paramagnetic relaxation and dipolar shifts, which provide unique and independent constraints on the distal residue orientations (Lecomte and La Mar, 1987; Emerson and La Mar, 1990a,b; Qin and La Mar, 1992; Qin et al., 1992, 1993a,b; Vyas et al., 1993; Zhao et al., 1995; Zhang et al., 1996). Target residues in contact with the heme, axial His and bound ligand, and their general location in the heme cavity, are depicted schematically in Fig. 1.

MATERIALS AND METHODS

Proteins

Mutagenesis and protein purification were performed as previously described (Springer and Sligar, 1987; Travaglini Allocatelli et al., 1994). Horse heart Mb was purchased from Sigma Chemical Co. (St. Louis, MO) and further purified by ammonium sulfate precipitation. Cyano-metMb (cyanide complex of ferric Mb) samples were prepared by adding potassium ferricyanide (protein:$K_3Fe(CN)_6$ = 1:1.5) to oxidize oxy-Mb and KCN to form the cyanide complex in either ^2H_2O or 90% ^1H_2O:10% ^2H_2O solution containing 50 mM NaCl, 10 mM KCN, 50 mM K_2HPO_4-KH_2PO_4 at pH 8.0. The final solution was ~2 mM in protein.

Cyanide dissociation rate constants from the reduced proteins were measured at 20°C in 0.2 M phosphate buffer (pH 7.0) by stopped-flow spectrophotometry with an Applied Photophysics DX.17Mv instrument (Leatherhead, England) as described elsewhere (Travaglini Allocatelli et al., 1993). Conditions after mixing were [Mb] = 2 μM, [KCN] = 1 mM, [$Na_2S_2O_4$] = 25 mM, and [methyl viologen] = 5 μM. Data analysis was carried out with a nonlinear fitting procedure.

^{1}H NMR measurements

All ^{1}H NMR spectra were collected on a GE Omega 500 MHz spectrometer. The WEFT (Gupta, 1976) pulse sequence was used to suppress the slowly relaxing diamagnetic envelope when necessary. Nonselective T_1 with ± 15% uncertainty for the resolved strongly relaxed protons were measured via inversion recovery experiment. Steady-state NOEs were recorded as described in detail previously (Emerson and La Mar, 1990a). The phase-sensitive 2D total correlation spectroscopy (TOCSY) (Braunschweiler and Ernst, 1983; Bax and Davis, 1985), NOESY (Jeener et al., 1979), and conventional n-type 2D correlation spectroscopy (MCOSY) (Bax, 1982) employed the method described by States et al. (1982) to

provide quadrature detection in the t_1 dimension. The spin-lock in TOCSY used the MLEV-17 scheme (Bax and Davis, 1985). Solvent suppression, when required, was achieved by direct saturation in the relaxation delay period. A total of 512 blocks were collected with two different spectral widths for all of the 2D experiments, 26.0 kHz to include all proton resonances, and 8.0 kHz to improve resolution for the unresolved diamagnetic envelope. A range of 128–256 scans were accumulated with repetition rate of 0.8 s^{-1} or 1.2 s^{-1} for each block, with free induction decays of 2048 complex points. The data were processed as previously described (Qin and La Mar, 1992); details are given in the figure captions.

Magnetic axes determination

The magnetic axes were determined as described in detail previously (Emerson and La Mar, 1990b; Rajarathnam et al., 1992, 1993; Qin et al., 1993a,b). Experimental dipolar shifts for the structurally conserved proximal side of the heme were used as input to search for the Euler rotation angles, $R(\alpha, \beta, \gamma)$, that transform the molecular pseudosymmetry coordinates (x', y', z', or r, θ', Ω'; Fig. 1), readily obtained from crystal coordinates, into magnetic axes, x, y, z, by minimizing the following global error function:

$$F/n = \sum| \delta_{dip}(obs) - \delta_{dip}(calc)F(\alpha, \beta, \gamma)|^2 \quad (1)$$

where

$$\delta_{dip}(calc) = -\frac{1}{3N} \cdot \left[\Delta\chi_{ax}(3\cos^2\theta' - 1)r^{-3} + \frac{3}{2}\Delta\chi_{rh}\sin^2\theta'\cos 2\Omega' r^{-3}\right] \quad (2)$$

and

$$\delta_{dip}(obs) = \delta_{DSS}(obs) - \delta_{DSS}(dia) \quad (3)$$

$\Delta\chi_{ax}$, $\Delta\chi_{rh}$ are axial and rhombic anisotropies, and $\delta_{DSS}(obs)$ is the observed chemical shift referenced to 2,2′-dimethyl-2-sila-5-pentane sulfonic acid (DSS). $\delta_{DSS}(dia)$ is the shift in the isostructural diamagnetic MbCO complex (Dalvit and Wright, 1987; Chiu, 1992), or is calculated for protons whose $\delta_{DSS}(dia)$ are not available by using the equation (Qin et al., 1993b)

$$\delta_{DSS}(dia) = \delta_{tetr} + \delta_{sec} + \delta_{rc} \quad (4)$$

where δ_{tetr} is the shift in an unfolded tetrapeptide; δ_{sec} is the shift of an amino acid proton typical for α-helices, β-strand, coils, etc. (Wishart et al., 1991); and δ_{rc} is the heme-induced ring current shift of the proton based on the WT coordinates by using the eight-loop model (Cross and Wright, 1985). The error function F/n in Eq. 1 was minimized over three parameters, α, β, γ, by using available $\Delta\chi_{ax}$ and $\Delta\chi_{rh}$ for WT metMbCN, or extended to all five parameters to yield both the Euler angles and anisotropies, as described in detail previously (Rajarathnam et al., 1992, 1993).

Structural modeling

The dipolar shifts of the residues expected to be perturbed in the point mutant relative to WT (i.e., distal side) and, in particular, the substituted E7, E10, and B10 residues, were analyzed to assess the nature of the perturbations. In each case, $\delta_{DSS}(dia)$ and $\delta_{dip}(calc)$ were calculated based on the proposed altered proton coordinates. The position of a perturbed distal residue was determined by minimizing a local error function for a selected set of protons (i.e., backbone for a helix or side-chain protons for a residue), as influenced by controlled local movements. This local error function, designated as F^*/n to distinguish it from that global error function in Eq. 1, is given by

$$F^*/n = \sum|\delta_{dip}(obs) - \delta_{dip}(\phi)|^2 \quad (5)$$

where $\delta_{dip}(\phi)$ represents the $\delta_{dip}(calc)$ as a function of a series of bond rotations for the side chain, as described in detail previously (Rajarathnam et al., 1993; Qin et al., 1993a,b), using the magnetic axes and anisotropies determined above. When available, the influence of paramagnetic relaxation, $T_1^{-1} \propto R_{Fe}^{-6}$, allowed estimates of R_{Fe} by using the relation

$$T_{1i}/T_{1j} = R_{Fe-i}^6/R_{Fe-j}^6 \quad (6)$$

where T_{1i} and R_{Fe-i}, for a reference proton with known R_{Fe-i}, allow an estimate of R_{Fe-j} with the determination of T_{1j}. The use of the His(F8) $N_\delta H$ (R_{Fe} = 5.0 Å) and heme methyl (R_{Fe} = 6.1 Å) as references provides the lower and upper bounds for R_{Fe-j}, respectively, as discussed in detail previously (Zhang et al., 1996). The steady-state NOE to a strongly relaxed proton i with T_{1i} is given by

$$\eta_{ji} = \sigma_{ij}T_{1i} \quad (7)$$

which yields an estimate for the i-j interproton distances, r_{ij}, via

$$\sigma_{ij} = -0.1(\hbar\gamma^2)^2 r_{ij}^{-6}\tau_c \quad (8)$$

where a correlation time, $\tau_c \approx 9$ ns, is assumed. The molecular modeling was carried out on a Silicon Graphics INDIGO ZX2 for the MbCO structure (Kuriyan et al., 1986), using the INSIGHT II program.

RESULTS

Cyanide dissociation rates

To obtain functional information on the cyanide derivative, we have measured cyanide dissociation rates from ferrous Mbs at 20°C and pH 7.0 for wild-type horse and sperm whale Mbs and for sperm whale H64Q-Mb, H64Q|T67R-Mb, and L29Y|H64Q|T67R-Mb. According to the scheme proposed by Bellelli et al. (1990), this reaction can be described as

$$Mb^{3+}(CN^-) \rightarrow Mb^{2+}(CN^-) \rightarrow Mb^{2+} + HCN \quad (9)$$

where protonation of bound cyanide is a key step in dissociation of the ligand introduced to account for the (small) pH dependence. If reduction of the iron is sufficiently rapid, the transient $Mb^{2+}(CN^-)$ complex becomes fully populated and the cyanide dissociation time course can be followed. With this experimental setup, the single-wavelength time courses, fitted to single exponentials, correspond to the

TABLE 1 Cyanide, carbon monoxide, and oxygen dissociation rate constants of wild-type and mutant Mbs and *P. equorum* Hb at pH 7.0, 20°C

	k_{CN^-}* (s^{-1})	k_{CO}# (s^{-1})	k_{O_2}# (s^{-1})
Horse Mb (WT)	0.09	0.017	10
Sperm whale			
WT	0.07	0.019	14
H64Q-Mb	0.04	0.012	130
H64Q|T67R-Mb	0.067	0.014	90,400
L29Y|H64Q|T67R-Mb	0.03	0.014	1
P. equorum Hb	0.011§	0.01¶	0.004¶

*Dissociation rate constant of the ferrous-cyanide complex.
#From Travaglini Allocatelli et al. (1994).
§From Antonini et al. (1994).
¶From Coletta et al. (1986).

second step in reaction 9. The results are given in Table 1, where they are also compared with previous data on oxygen and carbon monoxide dissociation rate constants for the same proteins. Differences with respect to cyanide dissociation among the various mutants are very small.

Resonance assignment

The ^{1}H NMR spectra of cyanomet complexes of H64Q|T67R-Mb and L29Y|H64Q|T67R-Mb in ^1H_2O are illustrated in Fig. 2, *A* and *B*, respectively (resolved labile protons lost in ^2H_2O are marked by an asterisk). A WEFT spectrum designed to emphasize strongly relaxed signals for L29Y|H64Q|T67R-metMbCN is shown in Fig. 2 *C*. Assignments deduced herein are given by the Fischer heme notation and the standard amino acid one-letter code. Heme cavity residues were pursued, to the degree possible, by backbone connectivities as standard in a diamagnetic protein (Wüthrich, 1986), with the remainder of the target residues assigned by detection of NOESY residue-heme and interresidue cross-peaks predicted by the WT MbCO crystal structure (Kuriyan et al., 1986), and the observation of

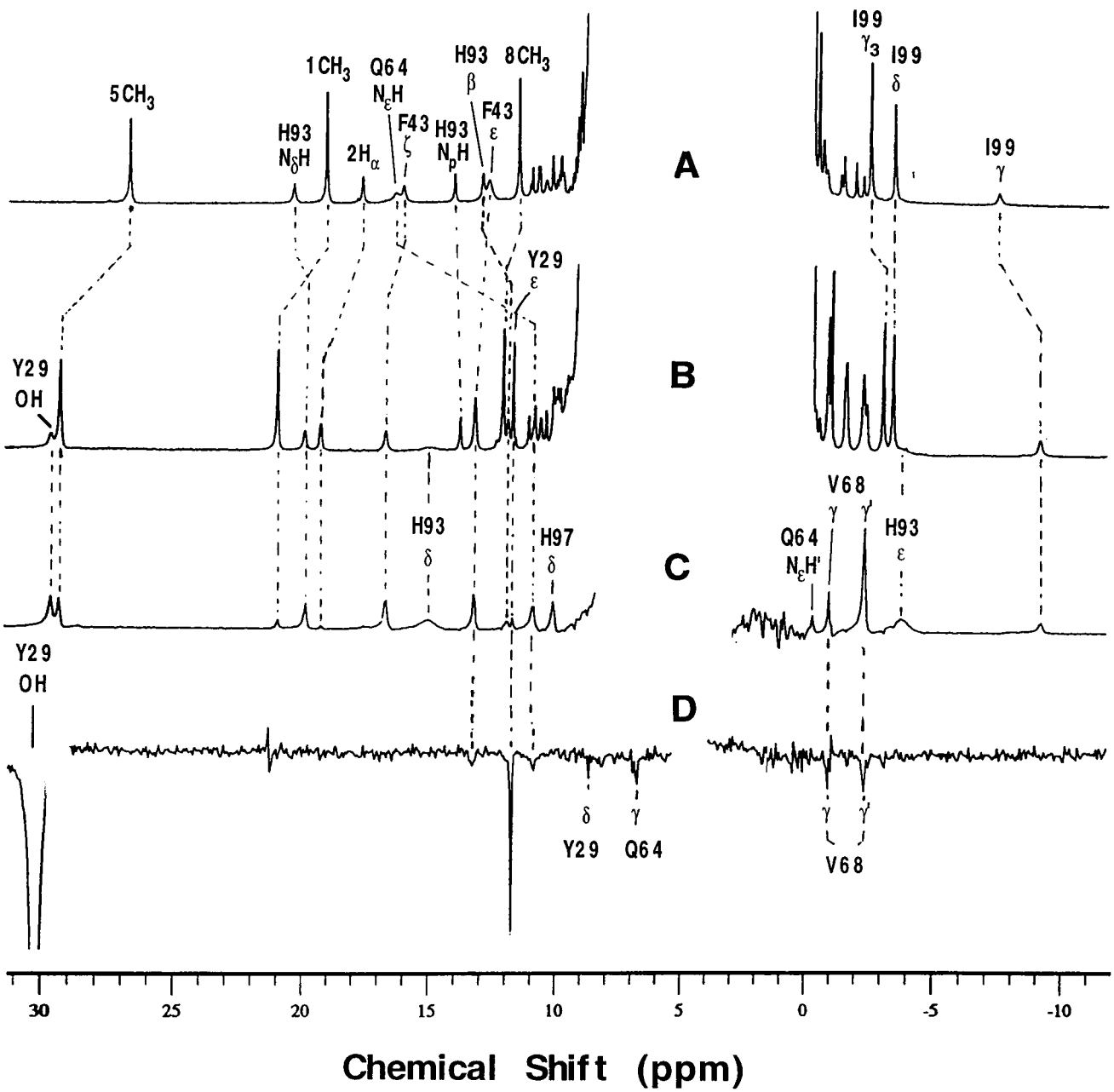

FIGURE 2 500-MHz ^{1}H NMR spectra in ^1H_2O at pH 8.0 and 25°C for (*A*) H64Q|T67R-metMbCN; (*B*) L29Y|H64Q|T67R-metMbCN; (*C*) WEFT spectrum for L29Y|H64Q|T67R-metMbCN; (*D*) steady-state NOE difference spectra of L29Y|H64Q|T67R-metMbCN upon irradiation of the Tyr29(B10) OH peak.

relaxation effects and/or sufficient TOCSY cross-peaks to uniquely identify the side chain. Representative ^1H 2D NMR data are shown only for L29Y|H64Q|T67R-metMbCN. The identification of hyperfine shifted and relaxed resonances was greatly facilitated by variable temperature studies to define unique scalar/dipolar connectivities as described previously (Qin and La Mar, 1992). The chemical shifts for all assigned resonances are listed in Table 2 for the heme, and in Table 3 for the target amino acid residues. T_1 values for predominantly paramagnetically influenced protons are given in parentheses.

Heme assignments

All heme protons were assigned in a standard manner by identifying the scalar connectivities for two vinyl and two propionate spin systems with significant hyperfine shifts, and their NOESY cross-peak pattern to strongly shifted but relatively weakly relaxed methyl peaks that do not themselves show a scalar cross-peak (Qin and La Mar, 1992); three of the heme methyl peaks are resolved. The meso-H signals were located as strongly relaxed signals with no scalar connectivity with dipolar contacts to adjacent methyls, vinyls, and/or propionates.

Sequence-specific assignments

Analysis of the low-field portion of the NOESY spectrum (Fig. 3 *B*) and the MCOSY spectrum (Fig. 3 *A*) of L29Y|H64Q|T67R-metMbCN in ^1H_2O reveals two short helical fragments with typical NH_i-NH_{i+1}, α_i-N_{i+1}, β_i-N_{i+1}, α_i-β_{i+3} connectivities. The scalar connectivities for some of the short side chains in segment I yield Leu_i-Ala_{i+1}-Z_{i+2}-AMX_{i+3}-AMX_{i+4}-Ala_{i+5}, which the sequence uniquely identifies as Leu89(F4)-Ala94(F9). AMX_{i+4} exhibits significant hyperfine shifts and a unique strong NOE to a strongly relaxed ($T_1 \approx 30$ ms) resolved labile proton characteristic of the axial His93(F8), with the latter proton arising from the side chain $N_\delta H$. All expected interresidue and residue-heme NOESY cross-peaks based on the WT NMR analysis were observed in the mutant (Emerson and La Mar, 1990a). The eight-member helical segment II is represented as $AMPTX_i$-Z_{i+1}-Val_{i+2}-AA′TT′MPX_{i+3}-Val_{i+4}-Z_{i+5}-Z_{i+6}-Ala_{i+7} (Z long chain), which the sequence identifies as Gln64(E7)-Ala71(E14), where significant hyperfine shifts for Gln64(E7), Arg67(E10), Val68(E11), and Ala71(E14)) greatly facilitated the identification of the complete spin systems. The conserved residues Val68(E11), Ala71(E14) exhibit the same heme contacts previously reported for WT. The NOESY contact for Val68(E11) $C_\alpha H$ to 8-CH_3 is slightly stronger relative to that to the 1-CH_3 than in WT, but the Ala71(E14) $C_\beta H_3$ contacts to both 1-CH_3 and 8-CH_3 are conserved.

A low-field, strongly relaxed ($T_1 \approx 20$ ms; $R_{Fe} = 4.4 \pm 0.2$ Å) labile proton exhibits NOEs (Fig. 4 *B*) to Gln64(E7) $C_\gamma H$, $C_\gamma H'$, and to an upfield, moderately relaxed ($T_1 \approx 50$ ms, $R_{Fe} \approx 5.3 \pm 0.3$ Å) labile proton (not shown), which identifies the Gln64(E7) $N_\epsilon H_2$. Four labile protons paired by 2D correlation spectroscopy (COSY), with one member of each pair exhibiting NOEs to $C_\delta Hs$, $C_\beta Hs$ of Arg67(E10), identify the guanidyl NH_2s for Arg67(E10). One pair of Arg67(E10) NHs exhibits NOESY cross-peaks to $C_\alpha H$, $C_\beta Hs$ of Gln64(E7). Hence the Arg67(E10) residue is oriented so as to provide contact between the guanidyl group and the distal Gln E7. All interresidue and residue-heme contacts are shown schematically in Fig. 1.

TABLE 2 ^1H NMR chemical shifts of heme resonances in sperm whale L29Y|H64Q|T67R- and H64Q|T67R-metMbCN*

Heme resonance	L29Y|H64Q|T67R-metMbCN	H64Q|T67R-metMbCN
1-CH_3	20.71	18.86
3-CH_3	5.17	5.58
5-CH_3	29.00	26.38
8-CH_3	11.84	11.30
2-H_α	18.99	17.44
2-$H_{\beta c}$	−1.87	−2.18
2-$H_{\beta t}$	−2.67	−2.72
4-H_α	5.64	#
4-$H_{\beta c}$	−1.81	−2.46
4-$H_{\beta t}$	−0.78	−1.56
6-$H_\alpha s$	9.74, 10.36	8.10, 9.54
6-$H_\beta s$	0.26, 2.42	0.47, 2.22
7-$H_\alpha s$	−0.63, 1.47	−1.02, 1.19
7-$H_\beta s$	0.40, 1.32	−0.28, 0.93
α-Meso-H	#	4.01
β-Meso-H	3.07	1.78
γ-Meso-H	5.47	#
δ-Meso-H	3.34	2.48

*Shifts in ppm referenced to DSS, in ^1H_2O, pH 8.0, at 25°C.
#Likely under the solvent signal.

Assignments by heme contacts

A complete Ile spin system in the upfield window exhibits all expected NOESY cross-peaks to the heme 3-CH_3, 4-vinyl, and 5-CH_3 characteristic for Ile99(FG5). A strongly relaxed ($T_1 \approx 10$ ms) low-field hyperfine shifted peak with an NOE to His93(F8) $C_\alpha H$ identifies the His97(FG3) $C_\delta H$, and an NOE to 6-$H_\alpha s$ locates the $C_\epsilon H$ as in WT (Emerson and La Mar, 1990a; Rajarathnam et al., 1993). Two other proximal heme contacts, Phe138(H15) and Leu104(G5), exhibit characteristic TOCSY peaks and the expected NOESY cross-peak to 1-CH_3, 2-H_α and 3-CH_3, respectively, with the latter also with the expected NOESY cross-peak to Ile99(FG5).

Distal side contacts (Fig. 1) include the aromatic ring of Phe43(CD1) with NOEs to 5-CH_3 and strongly relaxed ($T_1 \approx 20$ ms, $R_{Fe} \approx 4.4 \pm 0.2$ Å) H_ζ (and Phe33(B14) with NOESY cross-peak to Phe43(CD1)). A resolved and hyperfine shifted two-proton peak exhibits strong TOCSY/NOESY cross-peaks to another weakly low-field hyperfine shifted peak. The NOESY contacts for these two resonances to Phe43(CD1) $C_\epsilon Hs$, $C_\zeta H$, Gln64(E7) $C_\gamma Hs$, Val68(E11) $C_\beta H$, and Gly65(E8) NH uniquely identify the aromatic side chain of Tyr29(B10). A strongly relaxed ($T_1 \approx 11$ ms,

TABLE 3 ^{1}H NMR chemical shifts of heme cavity residues in sperm whale L29Y|H64Q|T67R-metMbCN and H64Q|T67R-metMbCN in ^1H_2O, pH 8.6, at 25°C*

Residue	Peak	L29Y|H64Q|T67R-metMbCN#	H64Q|T67R-metMbCN§
Tyr29(B10)	C_δHs	8.49	¶
	C_ϵHs	11.43(80)‖	
	OH	29.31(11)	
Phe43(CD1)	C_δHs	8.95	8.62
	C_ϵHs	12.95(36)	12.47
	C_ζH	16.44(20)	15.82
Gln64(E7)	N_pH	8.38	**
	C_αH	4.05	**
	C_βH	3.62	**
	C_βH′	3.08	**
	C_γH	6.56	9.93
	C_γH′	5.47	8.00
	N_ϵH	10.64(20)	16.12
	N_ϵH′	−0.48(50)	**
Arg67(E10)	N_pH	7.26	**
	C_αH	2.81	2.70
	C_βHs	0.41, −0.23	0.62, −0.86
	C_γHs	0.28, −0.12	0.68, 0.10
	C_δHs	1.56, 1.78	1.42, 1.85
	N_ηHs	9.85, 6.84	9.99, 6.85
	N_ηHs	9.67, 6.91	9.65, 6.91
Val68(E11)	N_pH	6.86	**
	C_αH	−1.80	−1.69
	C_βH	1.71	2.45
	$C_\gamma H_3$	−1.12	¶
	$C_\gamma' H_3$	−2.53	¶
Ala71(E14)	N_pH	6.28	6.08
	C_αH	3.58	3.47
	$C_\beta H_3$	0.03	−0.28
Leu89(F4)	N_pH	8.01	7.84
	C_αH	8.34	7.97
Ala90(F5)	N_pH	10.58	10.55
	C_αH	6.39	6.63
	$C_\beta H_3$	2.60	2.70
Gln91(F6)	N_pH	9.58	9.62
	C_αH	4.91	4.96
Ser92(F7)	N_pH	10.83	10.77
	C_αH	5.39	5.41
His93(F8)	N_pH	13.52	13.85
	C_αH	7.09	7.69
	C_βH	11.65	12.72
	C_βH′	6.34	7.97
	N_δH	19.61(26)	20.14
Ala94(F9)	N_pH	10.14	10.48
	C_αH	3.88	4.18
	$C_\beta H_3$	1.35	1.51
His97(FG3)	C_δH	9.82	10.22
	C_ϵH	6.71	6.56
Ile99(FG5)	C_αH	2.40	2.60
	C_βH	−0.04	1.03
	C_γH	−9.40(43)	−7.68
	C_γH′	−1.86	−0.90
	$C_\gamma H_3$	−3.30	−2.72
	$C_\delta H_3$	−3.68	−3.65

*Chemical shifts from DSS.
#Other assigned residues are the rings of Phe33(B14), 7.77, 8.10, 7.93 ppm; Phe46(CD4), 7.92, 7.79 ppm; and Phe138(H15), 6.99, 7.11, 7.39 ppm.
§Other assigned residues are the rings of Phe33(B14), 7.74, 8.01, 8.30 ppm; Phe46(CD4) 8.49, 7.92, 8.43 ppm; and Phe138(H15), 7.00, 7.08, 7.36 ppm.
¶Not assigned.
‖T_1, for resolved resonances (given in parenthesis), in ms; uncertainty ±15%.
**Leu29(B10) in H64Q|T67R-metMbCN, not assigned.

R_{Fe} = 4.1 ± 0.2 Å) labile proton exhibits NOEs (Fig. 2 *D*) to the C_ϵHs of Tyr29(B10), C_ϵHs of Phe43(CD1), C_βH, $C_\gamma H_3$s of Val68(E11), C_γH, and low-field side chain N_ϵH of Gln64(E7) (not shown). The latter ~−0.5% NOE, together with its 20-ms T_1, indicate a ~2.7 ± 0.2 Å distance (via Eqs. 7 and 8) between these two labile protons. The observed interresidue and heme-residue contacts are shown schematically in Fig. 1.

Determination of magnetic axes

The use of the observed dipolar shifts for a variety of conserved proximal residue protons as input to the three-parameter least-square searches (Eqs. 1 and 2) yielded α = 0°, β = 16.7°, γ = 40°, κ = 40° for L29Y|H64Q|T67R-metMbCN, and α = −10°, β = 12.9°, γ = 40°, κ = 30°, for H64Q|T67R-metMbCN, using the WT anisotropies $\Delta\chi_{ax} = 2.02 \times 10^{-9}$ m^3/mol, $\Delta\chi_{rh} = -0.54 \times 10^{-9}$ m^3/mol (Rajarathnam et al., 1993). The high quality of the fit for a representative input set for the triple mutant is shown in Fig. 5. Variation in the input data resulted in ~10° ranges in both α and κ, and only a 1° range for β. Extending the search to five parameters led to inconsequential changes in the angles and $\Delta\chi_{ax}$, $\Delta\chi_{rh}$, as was shown to be the case for numerous other distal point mutants of sperm whale Mb (Rajarathnam et al., 1993, 1994; Qin et al., 1993a,b).

Distal pocket structure of *YQR*-metMbCN

The Arg E10 side chain clearly exhibits small dipolar shifts, as reflected in the temperature dependence of its chemical shifts, but a search for the orientation that yields the optimum fit of δ_{dip}(obs) versus δ_{dip}(calc) proved futile in view of the relative insensitivity of the δ_{dip}(calc) for C_βH on χ_1, and C_γH on χ_2 angles. However, an orientation as found for Lys E10 in *Chironomus* Hb (Steigemann and Weber, 1979) or *Ascaris* Hb (Yang et al., 1995) yielded δ_{dip}(calc) consistent with δ_{dip}(obs), as shown in Fig. 7. Moreover, the orientation of the nonlabile protons allows the Arg E10 guanidyl group to place the $N_{\eta 1}H_2$ sufficiently close (within 3 Å) to the Gln E7 C_αH, $C_\beta H_2$ to rationalize the observed NOEs.

Insertion of the Tyr B10 side chain with the orientation exhibited by the Phe29(B10) residue in the L29F|H64Q-MbCO crystal structure (Quillin et al., 1993) resulted in δ_{dip}(calc), in excellent agreement with δ_{dip}(obs) for the ring. The large δ_{dip}(obs) and strong relaxation ($T_1 \approx 11$ ms, R_{Fe} = 4.2 ± 0.2 Å) for the Tyr29(B10) OH allow a simultaneous fit to both dipolar shift and relaxation, which defines the dihedral angle with the ring plane as ~115°. However, inspection of the resulting heme cavity structure reveals a strong steric interaction between the Tyr B10 oxygen and the ligated cyanide. Relieving this interaction by moving the B helix away from the iron by ~0.5 Å led to a similarly well-defined orientation for the Tyr29(B10) side

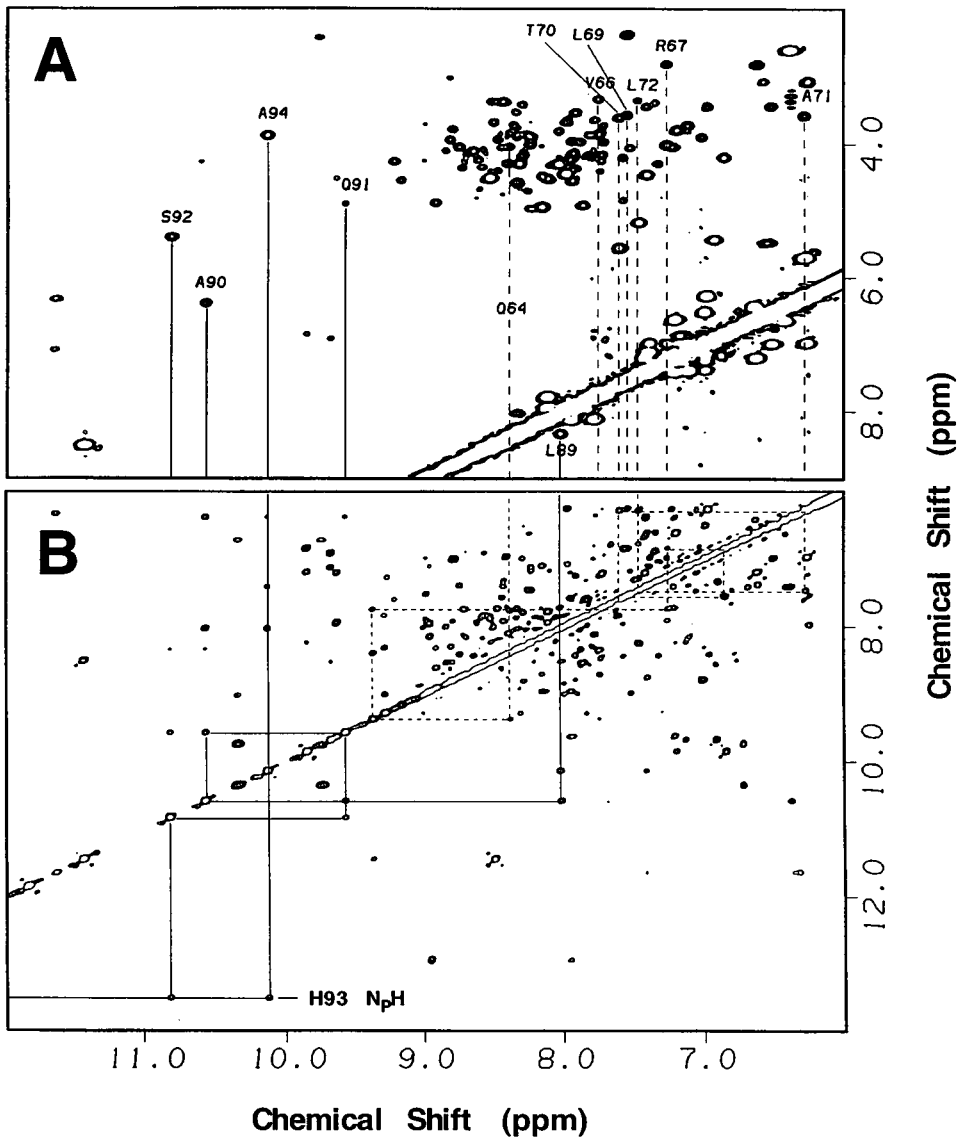

FIGURE 3 Fingerprint regions of the (*A*) MCOSY and (*B*) NOESY spectra (110 ms mixing time) for L29Y|H64Q|T67R-metMbCN in ^1H_2O at 25°C and pH 8.0. Two helical N_iH-$N_{i+1}H$ NOE sequences (I residues 89–94, II 64–71) are shown; the assigned N_iH-$C_\alpha H$ COSY peaks from the two helical segments are labeled by the one-letter code for the residue.

chain orientation, which is compatible with the placement of the remainder of the distal residues.

The orientation of Gln64(E7) was determined by constraining the terminal $N_\epsilon Hs$ to $R_{Fe} = 4.4 \pm 0.2$ Å for the low-field, and $R_{Fe} = 5.3 \pm 0.3$ Å for the upfield $N_\epsilon H$ and simultaneously optimizing the residue error function (Eq. 6) as a function of side-chain torsion angles. Because of the availability of strong structural constraints from both relaxation and δ_{dip}(obs), the spatial positions for the ~1.8-Å-separated $N_\epsilon Hs$ were determined first. On the one hand, because of the fact that the Gln64(E7) $N_\epsilon Hs$ must span the node in the dipolar field, δ_{dip}(obs) serves as a strong constraint on the location of the $N_\epsilon H_2$ group. However, the small net chemical shift for the low-field $N_\epsilon H$ reflects a near-cancellation of a significant low-field δ_{dip}(calc) and upfield heme ring current shifts (Eq. 4), which results in larger uncertainty in δ_{dip}(obs) for the low-field $N_\epsilon H$ than for the upfield $N_\epsilon H$. The $N_\epsilon Hs$ could satisfy both δ_{dip}(obs), T_1 constraints and the ~2.8-Å interproton distance between the low-field Gln64(E7) $N_\epsilon H$ and Tyr29(B10) OH obtained from the steady-state NOE (and T_1 for the former resonance) upon saturation of the latter resonance (Fig. 2 *D*). The optimized side-chain torsional angles that yielded a reasonable fit between δ_{dip}(obs) and δ_{dip}(calc) for all Gln64(E7) protons are shown in Fig. 6. The orientation of the three mutated residues in the L29Y|H64Q|T67R-metMbCN solution structure are depicted in Fig. 7 *A* and can be compared to the orientation of the same residues in the crystal structure of *Ascaris* HbO_2 (Fig. 7 *B*).

Direct evidence for one strong hydrogen bond to the bound cyanide in L29Y|H64Q|T67R-metMbCN is obtained from the effect of bulk solvent isotope composition on the heme hyperfine shifts, as has previously been reported for WT metMbCN (Lecomte and La Mar, 1987). Two heme 5-CH_3 peaks are resolved in ^1H_2O:^2H_2O solvent mixtures, with the relative intensity of the two 5-CH_3 signals directly proportional to the solvent ^1H:^2H composition, as illustrated in Fig. 8. This influence on the heme contact shift can be

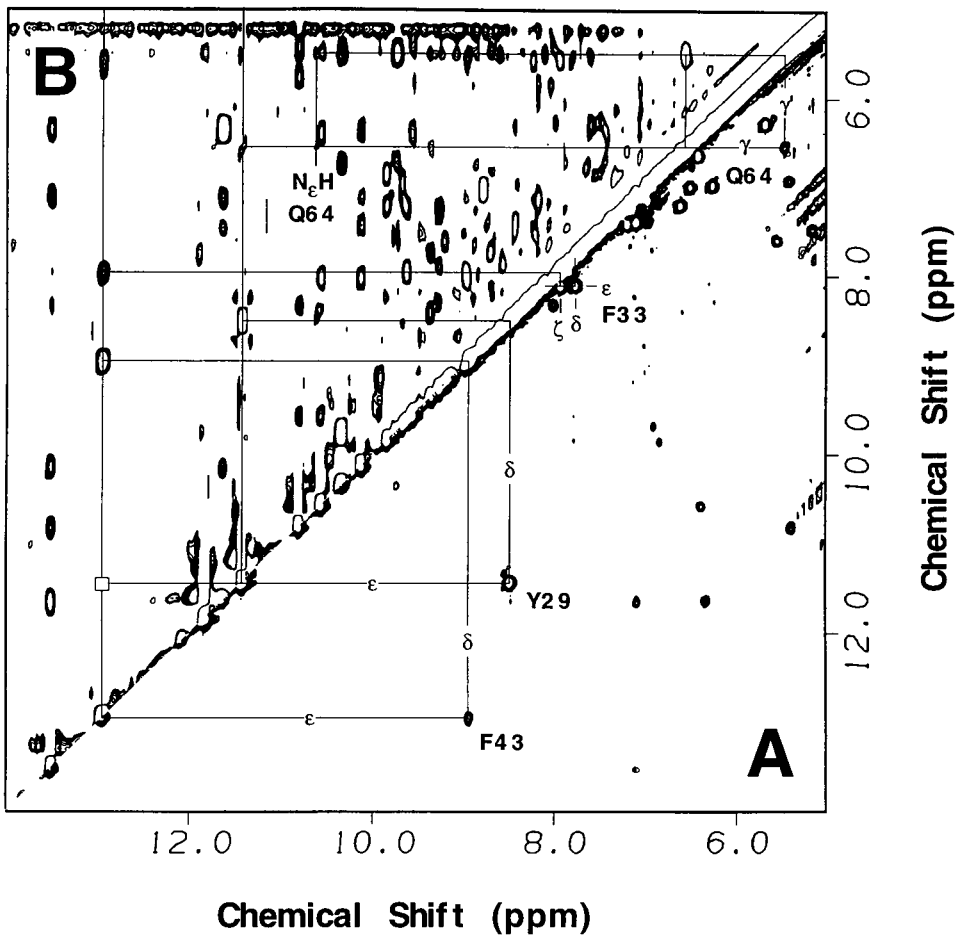

FIGURE 4 Resolved low-field portion of the 500-MHz ^1H NMR spectra for L29Y|H64Q|T67R-metMbCN in ^1H_2O, pH 8.0, at 25°C (*A*) MCOSY, and (*B*) NOESY map (40 ms mixing time) illustrating key dipolar contacts among distal pocket residues. NOEs observed at low contour levels are shown by boxes.

experienced only if there is a direct link between the heme iron and the labile proton. The splitting of the heme 5-CH_3 signals is 25 Hz, which is comparable to the 32 Hz observed due to the distal hydrogen bond by His64(E7) to the cyanide in WT metMbCN (Lecomte and La Mar, 1987).

Distal pocket structure of H64Q|T67R-metMbCN

The chemical shift for all hyperfine shifted residues for H64Q|T67R-metMbCN, and the resulting magnetic axes ($\alpha = -10°$, $\beta = 12.9°$, $\kappa \approx \alpha + \gamma = 30°$), are very similar to those reported previously for H64Q-metMbCN (Zhao et al., 1995). Moreover, modeling the Gln64(E7) orientation on the basis of the H64Q-MbCO crystal structure provided a good fit between δ_{dip}(obs) and δ_{dip}(calc) for Gln64(E7) (not shown). The observation of NOESY cross-peaks between the Gln64(E7) $C_\alpha H$, $C_\beta Hs$ with labile protons in the same manner as observed for L29Y|H64Q|T67R-metMbCN indicates that the Arg67(E10) is oriented as deduced above for the triple mutant.

DISCUSSION

Heme cavity structure

The combination of dipolar shift and paramagnetic relaxation constraints provides a well-defined structure for the distal heme pocket of both H64Q|T67R- and L29Y|H64Q|T67R-metMbCN. The proximal side structure typical of WT Mb is strongly conserved in all distal side mutants, as shown previously by both x-ray crystallography (Quillin et al., 1993; Zhao et al., 1995) and NMR (Rajarathnam et al., 1993, 1994; Qin et al., 1993a,b; Zhao et al., 1995). Hence the orientation of the magnetic axes and the magnitudes of the anisotropies determined herein are considered robust. The modeling of Tyr29(B10) presents something of a problem, because no direct NMR evidence is available to specify the position of the B helix. The movement of the B helix 0.5 Å away from the iron compared to WT is reasonable, but is only a qualitative indication of the likely response of helix B to steric interaction of its side-chain terminus with the bound ligand. A similar movement was observed in the L29F|H64Q-MbCO crystal structure, where the bulkier Phe29(B10) induces a small movement of the B-helix away from the iron (Zhao et al., 1995).

Hydrogen bonding in the distal pocket

The labile protons that participate in the distal hydrogen bonding network are observed directly by ^1H NMR in the cyanomet globins, and the combination of relaxation and dipolar shift constraints locates these putative hydrogen bond donors more accurately than can be inferred from the

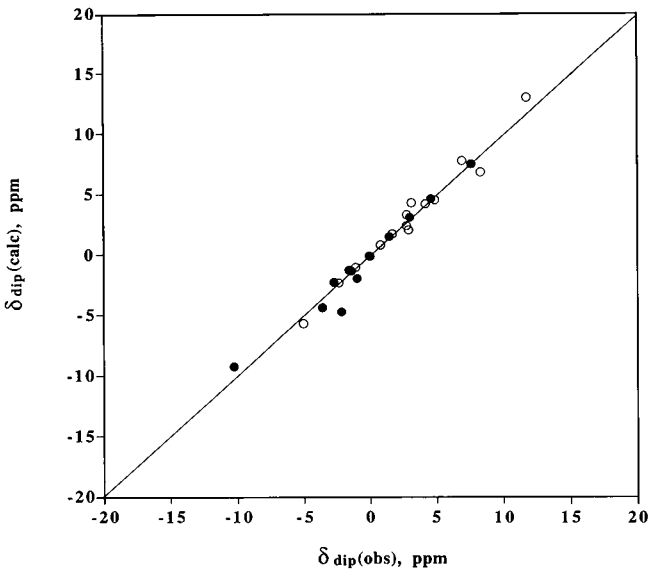

FIGURE 5 Plots of the δ_{dip}(calc) via Eq. 2, versus δ_{dip}(obs) via Eqs. 3 and 4 for the determined magnetic axes of L29Y|H64Q|T67R-metMbCN. The 14-input dipolar shifts for the determination of magnetic axis orientation and anisotropies are given by closed circles; the remainder of the resonances are shown by open circles. The solid line with unit slope represents the ideal fit.

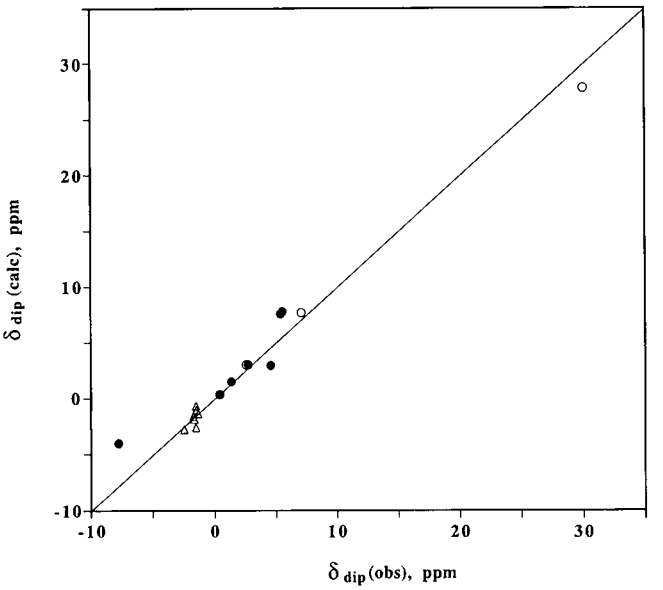

FIGURE 6 Plot of the δ_{dip}(calc) via Eq. 1 and δ_{dip}(obs) via Eqs. 3 and 4 for the determined magnetic axes for residues Tyr29(B10) (○), Gln64(E7) (●), and Arg67(E10) (△) for L29Y|H64Q|T67R-metMbCN, with the orientations determined by paramagnetic relaxation, dipolar shifts, and dipolar contacts.

location of the related heteroatoms in a crystal structure. The structures in Fig. 7 outline the orientations of the distal residues in contact with the bound cyanide in L29Y|H64Q|T67R-metMbCN and with dioxygen in *Ascaris* $HbIO_2$ (Fig. 7, *A* and *B*). The hydrogen bonding pattern observed in L29Y|H64Q|T67R-metMbCN is similar, but not identical to that reported for *Ascaris* HbO_2 (Yang et al., 1995).

In L29Y|H64Q|T67R-metMbCN, the positions of the Tyr29(B10) OH and the low field Gln64(E7) $N_\epsilon H$, dictated by the R_{Fe} from relaxation and δ_{dip}(calc), place both labile protons in van der Waals contact with the bound cyanide nitrogen, and hence identify them as possible hydrogen bond donors to the bound ligand. The orientation of the Tyr29(B10) OH is favorable for hydrogen bonding, because it is directed to the cyanide nitrogen lone pair; on the other hand, Gln64(E7) $N_\epsilon H$ is directed perpendicular to the lone pair, and it is probably not very effective in stabilizing the bound ligand. The low-field Gln64(E7) $N_\epsilon H$ is 3.7 Å from the Tyr29(B10) hydroxyl oxygen in L29Y|H64Q|T67R-metMbCN, and therefore a hydrogen bond between them is unlikely, which is at variance with what occurs for *Ascaris* $HbIO_2$ (Fig. 8 *B*); moreover, the relative orientation of these side chains is also unfavorable. On the other hand, the orientation of Arg67(E10) in L29Y|H64Q|T67R-metMbCN, consistent with the small δ_{dip}(obs) and the NOESY cross-peak between its guanidyl $N_\zeta H_2$ and the Gln64(E7) $C_\alpha H$, $C_\beta Hs$, places its guanidinium group at hydrogen bonding distance from the Gln64(E7) side-chain carbonyl group. Direct evidence for one hydrogen bond to the bound CN^- in L29Y|H64Q|T67R-metMbCN, comparable to that exercised by the His64(E7) $N_\epsilon H$ in WT metMbCN (Lecomte and La Mar, 1987), is obtained from solvent isotope effects on the heme (Fig. 8). In WT metMbCN, a comparable resolution of separate heme methyl signals was observed and the averaging of the environments at alkaline pH was traced directly to the lability of the distal His64(E7) $N_\epsilon H$ (Lecomte and La Mar, 1987). In L29Y|H64Q|T67R-metMbCN, the "splitting" of the 5-CH_3 peaks in 1:1 ^1H_2O:^2H_2O is maintained to pH 10, which is consistent with the slower exchange of the Tyr29(B10)OH, as also manifested in the absence of saturation transfer from bulk solvent at alkaline pH. A strong H bond between the distal Tyr(B10) in *Ascaris* HbO_2 has been directly established by resonance Raman spectroscopy (Huang et al., 1996).

Cyanide dissociation

The kinetics of cyanide dissociation from the ferrous form of Mb (Table 1) indicates that WT sperm whale Mb and the three mutants have essentially the same rate constant (within a factor of ~2). The same was observed for the carbon monoxide dissociation rate constant, whereas the oxygen dissociation rate constant varies considerably (>100 fold) when Gln64(E7) and Tyr29(B10) alone, or in combination, are present (Travaglini Allocatelli et al., 1994, and Table 1). These results show that the stabilizing contribution of Tyr29(B10) in L29Y|H64Q|T67R-Mb is only effective with oxygen. We wish to comment on this observation.

The rate-limiting step in the intrinsically slow dissociation of CN^- and CO from iron(II) is to be assigned to the thermal rate of breaking of the Fe-C bond. The increase in

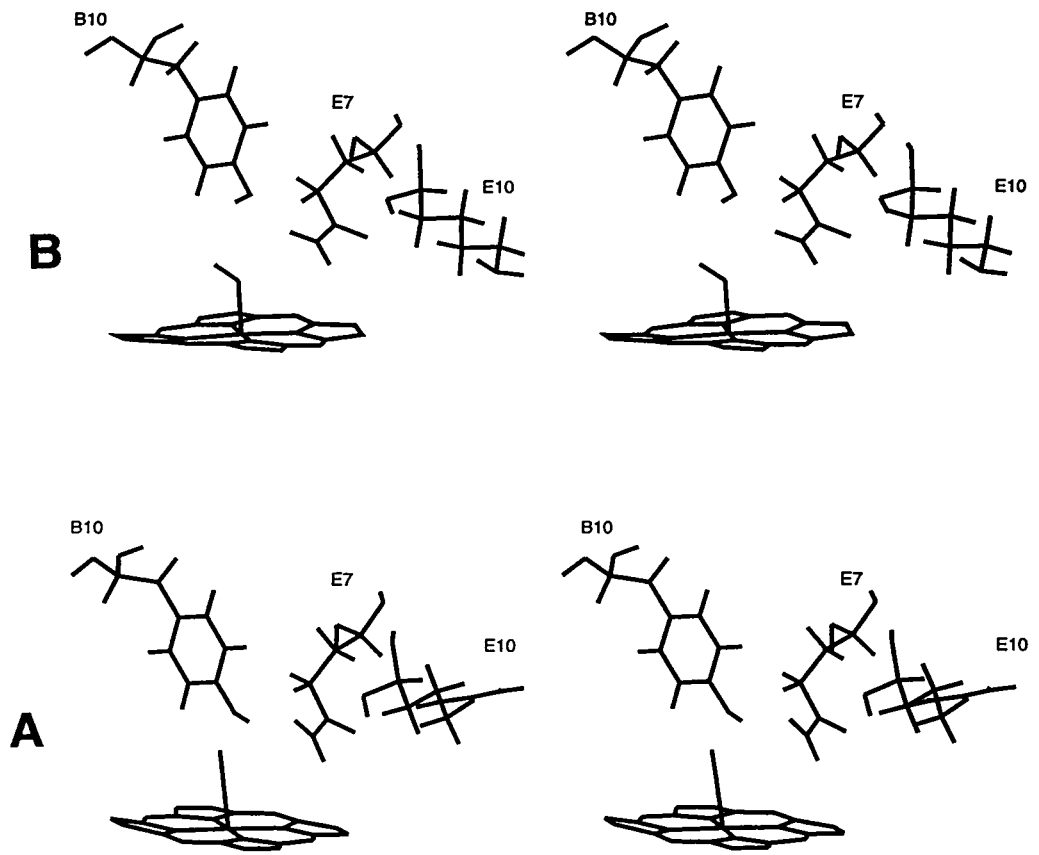

FIGURE 7 Stereo view of the distal hydrogen-bond network involving the ligand, Tyr(B10), Gln(E7), and Lys/Arg(E10) for (*A*) L29Y|H64Q|T67R-metMbCN and (*B*) *Ascaris* $HbIO_2$.

hydrogen bonding capability in L29Y|H64Q|T67R-Mb with respect to wild-type Mb has no effect on the CO dissociation rate, consistent with what is observed for other sperm whale mutants in which the distal HisE7 has been removed (Springer et al., 1994). However, cyanide dissociation from the ferrous heme is peculiar in so far as a key step in dissociation involves protonation of CN^-, either from a distal residue (His E7) or from the bulk solvent (Bellelli et al., 1990); its rate is also unaffected in these mutants, because the total number of proton donors in the pocket is unchanged (all mutants lack HisE7) and none of the mutants have severely altered solvent accessibility. We conclude that, like CO, cyanide dissociation is rate limited by the Fe^{2+}-C bond breaking, and any contribution of distal H-bond(s) to the rate of dissociation has a marginal effect.

Relevance to O_2 dissociation

As far as oxygen is concerned, the dissociation rate constant reflects both the Fe-O_2 bond breaking and ligand escape from the protein matrix. Because the intrinsic rate for the iron-O_2 bond dissociation is very fast ($k > 10^3\ s^{-1}$) in the absence of H-bond donors (Springer et al., 1994), hydrogen bond(s) on the distal site will help to hold the dissociated ligand in the pocket and will have a substantial effect on the overall rate of dissociation, making O_2 unique; in fact, a role for the distal Gln(E7) and Tyr(B10) can be seen only for O_2 (Table 1). Why, then, is the rate constant for O_2 dissociation in L29Y|H64Q|T67R-Mb (although slower than WT) still 200 times faster than *Ascaris* Hb? The presence of a hydrogen bond between the Tyr B10 hydroxyl and the bound cyanide (as seen above by NMR) indicates that this is the stabilizing contribution responsible for slowing down O_2 dissociation in L29Y|H64Q|T67R-Mb; however, the marginal or absent interaction between Gln(E7) and bound CN^-, the absence of the interresidue Gln(E7)-Tyr(B10) hydrogen bond that stabilizes Tyr(B10) in a favorable orientation, and the need to postulate a ~0.5-Å displacement of the B helix away from the iron likely all contribute to a less stable H-bonding network, and hence a much faster O_2 off rate in L29Y|H64Q|T67R-Mb relative to *Ascaris* Hb. In this scenario, the hydrogen bond between the guanidinium group of Arg(E10) and the side-chain carbonyl of Gln(E7) may stabilize the latter in an orientation that compromises its ability to hydrogen bond to both the ligand and Tyr(B10).

CONCLUSIONS

The results presented above provide structural support for the successful introduction of an alternative hydrogen bond

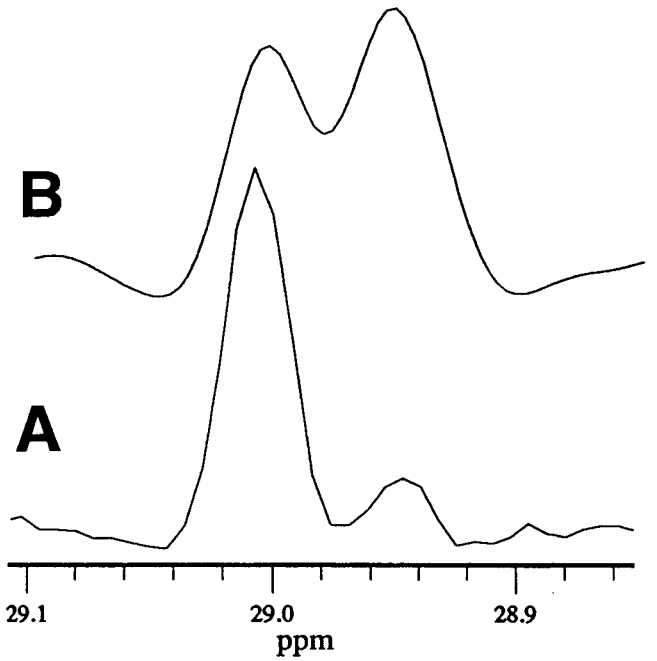

FIGURE 8 Expanded portion of the 500 MHz ^1H NMR spectrum of L29Y|H64Q|T67R-metMbCN in ^1H_2O, pH 8.0, at 25°C, showing the split heme 5-CH_3 signal in (*A*) 90% ^1H_2O:10% ^2H_2O; and (*B*) 50% ^1H_2O:50% ^2H_2O. Note that two separate 5-CH_3 peaks are resolved, the relative intensities of which parallel the solvent ^1H:^2H isotope composition, thereby establishing the presence of one relatively strong hydrogen bond between a distal residue and bound cyanide (Lecomte and La Mar, 1987).

to the iron ligand in engineered sperm whale Mb. This novel interaction exerts different effects on the stabilization of the three different ligands O_2, CO, and CN^-. The hypothesis outlined above suggests that shifting one hydrogen bond from Arg(E10)-Gln(E7) to Gln(E7)-Tyr(B10) by mutagenesis of Arg(E10) could result in further stabilization of the bound oxygen.

The authors are indebted to B. Nguyen for experimental assistance.

The research was supported by grants from the National Institutes of Health (HL 16087) and Ministero dell'Universitá e Ricerca Scientifica e Technologica (40% Liverprotein), Istituto Pasteur Fondazione Cenci Bolognette (Rome, Italy), and Centro Nazionale Ricerce (CTB95.02874.14).

REFERENCES

Antonini, G., A. Bellelli, A. Concetti, G. Falcioni, and M. Brunori. 1994. Cyanide dissociation from the hemoglobin of *Parascaris equorum*. *Biochim. Biophys. Acta.* 1205:252–257.

Antonini, E., and M. Brunori. 1971. Hemoglobin and Myoglobin in Their Reaction with Liquids. Elsevier, Amsterdam.

Bax, A. 1982. Two-Dimensional Nuclear Magnetic Resonance in Liquids. Delft University Press, Dordrecht, Holland.

Bax, A., and D. G. Davis. 1985. Mlev-17-based two-dimensional homonuclear magnetization transfer spectroscopy. *J. Magn. Reson.* 65: 355–360.

Bellelli, A., G. Antonini, M. Brunori, B. A. Springer, and S. G. Sligar. 1990. Ligand binding to a hemoprotein lacking the distal histidine. *J. Biol. Chem.* 265:18898–18901.

Bolognesi, M., A. Coda, F. Grigerio, G. Gatti, P. Ascenzi, and M. Brunori. 1990. X-ray crystal structure of the fluoride derivative of *Aplysia limacina* ferric myoglobin at 2.0 Å resolution. *J. Mol. Biol.* 213:621–625.

Bolognesi, M., S. Onesti, G. Gatti, A. Coda, P. Ascenzi, A. Giacometti, and M. Brunori. 1989. *Aplysia limacina* myoglobin crystallographic analysis at 1.6 Å resolution. *J. Mol. Biol.* 205:529–544.

Braunschweiler, L., and R. R. Ernst. 1983. Coherence transfer by isotropic mixing: application to proton correlation spectroscopy. *J. Magn. Reson.* 53:521–528.

Bunn, H. F., and B. G. Forget. 1986. M hemoglobins. *In* Hemoglobin Molecules, Genetic and Clinical Aspects. W. B. Saunders, Philadelphia. 623–637.

Carver, T. E., R. E. Brantley, Jr., E. W. Singleton, R. M. Arduini, M. L. Quillin, G. N. Phillips, Jr., and J. S. Olson. 1992. A novel site-directed mutant of myoglobin with an unusually high O_2 affinity and low autooxidation rate. *J. Biol. Chem.* 267:14443–14450.

Chiu, M. L. 1992. Structure and dynamics of myoglobin and its mutants. Ph.D. thesis. University of Illinois, Urbana, IL.

Coletta, M., G. Falcioni, A. Concetti, F. Ascoli, and M. Brunori. 1986. Ligand-dependent behavior of the hemoglobin from the ascarid *Parascaris equorum*. *Biochim. Biophys. Acta.* 870:169–175.

Cross, K. J., and P. E. Wright. 1985. Calibration of ring-current models for the heme ring. *J. Magn. Reson.* 64:220–231.

Cutruzzolá, F., C. Travaglini Allocatelli, A. Brancaccio, and M. Brunori. 1996. *Aplysia limacina* myoglobin cDNA cloning—an alternative mechanism of oxygen stabilization as studied by active-site mutagenesis. *Biochem. J.* 314:83–90.

Dalvit, C., and P. E. Wright. 1987. Assignment of resonances in the ^1H nuclear magnetic resonance spectrum of the carbon monoxide complex of sperm whale myoglobin by phase-sensitive two-dimensional techniques. *J. Mol. Biol.* 194:313–327, 329–339.

Davenport, H. E. 1949. Hemoglobins of *Ascaris lumbricoides*. *Proc. R. Soc. Lond. Biol.* 136:255–270.

De Baere, I., M. F. Perutz, L. Kiger, M. Marden, and C. Poyart. 1994. Formation of two hydrogen bonds from the globin to the heme-linked oxygen molecule in *Ascaris* hemoglobin. *Proc. Natl. Acad. Sci. USA.* 91:1594–1597.

Dene, H., M. Goodman, and A. E. Romero-Herrera. 1980. The amino acid sequence (Elephas maximus) myoglobin and the phylogen of Proboscidea. *Proc. R. Soc. Lond. Biol.* 207:111–127.

Emerson, S. D., and G. N. La Mar. 1990a. Solution structural characterization of cyano met-myoglobin: resonance assignment of heme cavity residues by 2D NMR. *Biochemistry.* 29:1545–1555.

Emerson, S. D., and G. N. La Mar. 1990b. NMR determination of the orientation of the magnetic susceptibility tensor in cyano met-myoglobin: a new probe of steric tilt of bound ligand. *Biochemistry.* 29:1556–1566.

Gibson, Q. H., and M. H. Smith. 1965. Rates of reactions of *Ascaris* hemoglobins with ligands. *Proc. R. Soc. Lond. Biol.* 163:206–214.

Gupta, R. K. 1976. Dynamic range problem in Fourier transform NMR. Modified WEFT pulse sequence. *J. Magn. Reson.* 24:461–465.

Huang, S., J. Huang, A. P. Kloek, D. E. Goldberg, and J. M. Friedman. 1996. Hydrogen bonding of tyrosine B10 to heme-bound oxygen in *Ascaris* hemoglobin. Direct evidence of UV resonance Raman spectroscopy. *J. Biol. Chem.* 271:958–962.

Jeener, J., B. H. Meier, P. Bachmann, and R. R. Ernst. 1979. Investigation of exchange processes by two-dimensional NMR spectroscopy. *J. Chem. Phys.* 71:4546–4553.

Kloek, A. P., J. Yang, F. S. Mathews, C. Frieden, and D. E. Goldberg. 1994. The tyrosine-B10 hydroxyl is crucial for oxygen avidity of *Ascaris* hemoglobin. *J. Biol. Chem.* 269:2377–2379.

Kuriyan, J., S. Wilz, M. Karplus, and G. A. Petsko. 1986. X-ray structure and refinement of carbon-monoxy (Fe-II)-myoglobin at 1.5 Å resolution. *J. Mol. Biol.* 192:133–154.

Lecomte, J., and G. N. La Mar. 1987. ^1H NMR probe for hydrogen bonding of distal residues to bound ligands in heme proteins: isotope effect on heme electronic structure of myoglobin. *J. Am. Chem. Soc.* 109: 7219–7220.

Li, T., M. L. Quillin, G. N. Phillips, Jr., and J. S. Olson. 1994. Structural determinants of the stretching frequency of CO bound to myoglobin. *Biochemistry.* 33:1433–1446.

Moens, L., J. Vanfleteren, Y. Van de Peer, K. Peeters, O. Kapp, J. Czelusniak, M. Goodman, M. Blaxter, and S. Vinogradov. 1996. Globins in nonvertebrate species—dispersal by horizontal gene transfer and evolution of the structure-function relationships. *Mol. Biochem. Evol.* 13:324–333.

Olson, J. S., A. J. Mathews, R. J. Rohlfs, B. A. Springer, K. D. Egeberg, S. J. Sligar, J. Tame, J. P. Renaud, and K. Nagai. 1988. The role of the distal histidine in myoglobin and hemoglobin. *Nature.* 336:265–266.

Perutz, M. F. 1989. Myoglobin and haemoglobin: role of distal residues in reactions with haem ligands. *Trends Biochem. Sci.* 14:42–44.

Philips, S. E. V., and B. P. Schoenborn. 1981. Neutron diffraction reveals oxygen-histidine hydrogen bond in oxymyoglobin. *Nature.* 292:81–82.

Qin, J., and G. N. La Mar. 1992. Complete sequence-specific ^{1}H NMR resonance assignment of hyperfine-shifted residues in the active site of a paramagnetic protein: application to *Aplysia* cyano-metmyoglobin. *J. Biomol. NMR.* 2:597–618.

Qin, J., G. N. La Mar, F. Ascoli, M. Bolognesi, and M. Brunori. 1992. Solution ^{1}H NMR determination of hydrogen bonding of the E10 (66) Arg side chain to the bound ligand in *Aplysia* cyano-met myoglobin. *J. Mol. Biol.* 224:891–897.

Qin, J., G. N. La Mar, F. Ascoli, and M. Brunori. 1993a. Solution NMR determination of active site structure for a paramagnetic protein: cyano-met *Aplysia* Mb. *J. Mol. Biol.* 231:1009–1023.

Qin, J., G. N. La Mar, F. Cutruzzolá, C. Travaglini Allocatelli, A. Brancaccio, and M. Brunori. 1993b. Solution ^{1}H NMR determination of the distal pocket structure of cyanomet complexes of genetically engineered sperm whale myoglobin His 64(E7) → Val, Thr 67(E10) → Arg. The role of distal hydrogen bonding by Arg 67 (E10) in modulating ligand tilt. *Biophys. J.* 65:2178–2190.

Quillin, M. L., R. M. Arduini, J. S. Olson, and G. N. Phillips. 1993. High-resolution crystal structures of distal histidine mutants of sperm whale myoglobin. *J. Mol. Biol.* 234:140–155.

Rajarathnam, K., G. N. La Mar, M. L. Chiu, and S. G. Sligar. 1992. Determination of the orientation of the magnetic axes of the cyano-met complexes of point mutants of myoglobin by solution ^{1}H NMR: influence of His E7 → Gly and Agr CD3 → Gly substitutions. *J. Am. Chem. Soc.* 114:9048–9058.

Rajarathnam, K., J. Qin, G. N. La Mar, M. L. Chiu, and S. G. Sligar. 1993. Solution structure determination of the heme cavity in the E7 His → Val cyano-met myoglobin point mutant based on the ^{1}H NMR detected dipolar field of the iron: evidence for contraction of the heme pocket. *Biochemistry.* 32:5670–5680.

Rajarathnam, K., J. Qin, G. N. La Mar, M. L. Chiu, and S. G. Sligar. 1994. Correlation between the steric bulk of the distal E7 and E11 residues and the tilt of the Fe-CN unit in cyanometmyoglobin as determined by NMR from the orientation of the magnetic axes in single and double point mutants. *Biochemistry.* 33:5493–5501.

Shaanan, B. 1983. Structure of human oxyhemoglobin at 2.1 Å resolution. *J. Mol. Biol.* 171:31–59.

Sharma, V. S., T. G. Traylor, R. Gardiner, and H. Mizukami. 1987. Reaction of nitric oxide with heme proteins and model compounds of hemoglobin. *Biochemistry.* 26:3837–3843.

Springer, B. A., and S. G. Sligar. 1987. High-level expression of sperm whale myoglobin in *Escherichia coli. Proc. Natl. Acad. Sci. USA.* 84:8961–8965.

Springer, B. A., S. G. Sligar, J. S. Olson, and G. N. Phillips, Jr. 1994. Mechanisms of ligand recognition in myoglobin. *Chem. Rev.* 94: 699–714.

States, D. J., R. A. Haberkorn, and D. J. Reuben. 1982. A two-dimensional nuclear Overhauser experiment with pure absorption phase in four quadrants. *J. Magn. Reson.* 48:286–292.

Steigemann, W., and E. Weber. 1979. Structure of erythrocruorin in different ligand states refined at 2.0 Å resolution. *J. Mol. Biol.* 127: 309–338.

Travaglini Allocatelli, C., F. Cutruzzolá, A. Brancaccio, M. Brunori, J. Qin, and G. N. La Mar. 1993. Structural and functional characterization of sperm whale myoglobin mutants: role of arginine (E10) in ligand stabilization. *Biochemistry.* 32:6041–6049.

Travaglini Allocatelli, C., F. Cutruzzolá, A. Brancaccio, B. Vallone, and M. Brunori. 1994. Engineering *Ascaris* hemoglobin oxygen affinity in sperm whale myoglobin—role of Tyrosine B10. *FEBS Lett.* 352:63–66.

Vyas, K., K. Rajarathnam, L. P. Yu, S. D. Emerson, and G. N. La Mar. 1993. ^{1}H NMR investigation of the heme cavity of elephant (E7 Gln) metMbCN: evidence for a B-helix phenylalanine interaction with bound ligand. *J. Biol. Chem.* 268:14826–14835.

Wishart, D. S., B. D. Sykes, and F. M. Richards. 1991. Relationship between nuclear magnetic resonance chemical shift and protein secondary structure. *J. Mol. Biol.* 221:311–333.

Wüthrich, K. 1986. NMR of Proteins and Nucleic Acids. Wiley-International, New York.

Yang, J., A. Kloek, D. E. Goldberg, and F. S. Mathews. 1995. The structure of *Ascaris* hemoglobin domain I at 2.2 angstrom resolution—molecular features of oxygen avidity. *Proc. Natl. Acad. Sci. USA.* 92:4224–4228.

Zhang, W., G. N. La Mar, and K. Gersonde. 1996. ^{1}H NMR structure of the heme cavity in the low-affinity state for the allosteric monomeric cyano-met hemoglobins from *Chironomus thummi thummi*: comparison to the crystal structure. *Eur. J. Biochem.* 237:841–853.

Zhao, X., K. Vyas, B. D. Nguyen, K. Rajarathnam, G. N. La Mar, T. Li, G. N. Phillips, Jr., R. F. Eich, J. S. Olson, J. Ling, and D. F. Bocian. 1995. A double mutant sperm whale myoglobin mimics the structure and function of elephant myoglobin. *J. Biol. Chem.* 270:20763–20774.